East European Journal of Physics. 3. 456-469 (2026)
DOI:10.26565/2312-4334-2026-3-41 ISSN 2312-4334

A MODIFIED RUNGE–KUTTA AND COMPACT SPATIAL SCHEME FOR DARCY-FORCHHEIMER PRANDTL–EYRING FLUID FLOW OVER A RIGA PLATE

Yasir Nawaz[1]*, Muhammad Shoaib Arif[2], Muavia Mansoor[3], Kamal Abodayeh[2]
[1]*Department of Mathematics, Faculty of Engineering and Computing, National University of Modern Languages (NUML), Islamabad, 44000, Pakistan*
[2]*Department of Mathematics and Sciences, College of Sciences and Humanities, Prince Sultan University, Riyadh, 11586, Saudi Arabia*
[3]*Department of Mathematics, University of Wah, Wah Cantt 47040, Pakistan*
**Corresponding Author email: yasir.nawaz@numl.edu.pk*
Received April 30, 2026; revised July 3, 2026; accepted July 12, 2026

A modification of existing third order Runge-Kutta method, is proposed. The scheme is explicit, and its first stage consists of a nonstandard denominator, while the last two stages are the same as those of the Runge-Kutta method. For discretizing space-dependent terms, a compact, high-order scheme is employed. The proposed scheme with spatial discretization is employed to find the stability condition of the proposed scheme. The scheme is applied to a dimensionless model in the form of partial differential equations for the slip flow of a non-Newtonian fluid over a Riga plate with heat and mass transfer. Different types of graphs are obtained using the proposed scheme for velocity, temperature, and concentration profiles. Some of the results obtained by the proposed scheme are compared with those obtained by the numerical solution using the MATLAB PDEPE solver. The scheme is also compared with an existing third-order Runge-Kutta scheme, and it produces more accurate results than the existing scheme at specific time and space step sizes.
Keywords: *Hybrid Scheme; Stability; Convergence; Slip Flow; Eyring-Prandtl Fluid*

INTRODUCTION

There exist variour methods that can be used to solve differential equations arise in phenomenon of flow over plates. Some analyrical and numerical methods can be used for solving ordinary diferential equaitons. Since, ordinary differential equatiuons contains one inpendent variable, so only one method can be used to solve these equations. But partial differential equations contain more than one independent variables, so two or more method must be chosen or contructed to solve thsese equations. Analytial methods [1] can be used to solve different type of equaitons but these methods may consume more time to converge because they deal with algebraic expression. So, numerical methods [2] can be chosen to solve different type of differetal equations. The numerical simulation of nonlinear differential systems arising in fluid mechanics, porous-media transport, and non-Newtonian rheology relies heavily on robust time-integration techniques. Among these, Runge–Kutta (RK) methods have remained central because of their simplicity, accuracy, and adaptability to a wide range of ordinary differential equation (ODE) and semi-discrete partial differential equation (PDE) problems. Classical expositions of RK theory by Butcher [3] and by Hairer & Wanner [4] establish stability categories (A-, L-, and B-stability) and provide the foundational convergence results through Dahlquist-type analyses. However, for stiff or strongly nonlinear systems—such as those produced by convection–diffusion–reaction models, porous-media flows, or high-nonlinearity non-Newtonian fluids—the standard explicit RK methods can become inefficient due to restrictive timestep bounds. This limitation has motivated the development of *modified* or *stabilized* RK schemes with enlarged stability regions and improved nonlinear contractivity properties.

Stabilized explicit RK methods, including Chebyshev-based schemes and extended-stability formulations, have been studied extensively for diffusion-dominated PDEs and stiff ODEs, as documented in works on stabilized RK theory [5-9]. These methods achieve extended stability along the negative real axis—crucial for method-of-lines discretizations of parabolic and convection–diffusion PDEs. Parallel efforts have analyzed RK stability, nonlinearity-preserving properties, and algebraic stability conditions essential for stiff systems [10–12]. A recent contribution by Hu [7] proposed a modified RK method with an enlarged stability domain and improved convergence characteristics, illustrating the modern trend toward structure-preserving and stiffness-aware RK design.

These numerical advancements are directly relevant to fluid-mechanical systems governed by *mixed convection Darcy–Forchheimer flow*, especially when involving *non-Newtonian Prandtl–Eyring (Eyring–Prandtl) fluids*. Classical studies on Darcy–Forchheimer convection in porous media, such as those by Shenoy [13], demonstrate that porous-inertia corrections introduce nonlinearities that significantly affect velocity profiles, heat transfer, and boundary-layer structure. More recent works by Shah et al. [14] and Chaudhary [15] show that Eyring–Prandtl rheology further complicates the governing equations due to nonlinear shear-rate dependencies, requiring stable time-integration and careful numerical formulations. Comprehensive modeling of Eyring–Prandtl fluids and their thermo-physical behavior is provided by Ullah et al. [16] and Baidya [17], highlighting rheological sensitivity and the necessity for robust numerical treatment.

Cite as: Y. Nawaz, M.Sh. Arif, M. Mansoor, K. Abodayeh, East Eur. J. Phys. 3, 456 (2026), https://doi.org/10.26565/2312-4334-2026-3-41

In addition, Riga plates—electromagnetically actuated surfaces composed of alternating electrodes and magnets—introduce localized Lorentz forces capable of accelerating or decelerating the near-wall region. Their applications in MHD and hybrid-fluid systems have been studied in numerical and experimental contexts, including magnetite nanofluids [20] and hybrid Riga-plate-induced flow systems [21]. These works show that the interaction between electromagnetic forcing and fluid rheology generates intricate nonlinear momentum dynamics. Because Riga plate forcing modifies the boundary-layer structure, it introduces additional stiffness in the resulting ODE system after similarity or quasi-similarity transformation.

Furthermore, viscous dissipation, a key component in high-viscosity or high-velocity non-Newtonian flows, contributes to a strong coupling between the momentum and energy equations. Its importance in porous-media and non-Newtonian flows is demonstrated in studies by Awais et al. [18] and Ajibade et al. [19], where dissipation significantly alters temperature fields, enhances nonlinearity, and contributes to stiffness in the governing PDE system.

Taken together, mixed-convection Darcy–Forchheimer flow of an Eyring–Prandtl fluid over a Riga plate with viscous dissipation forms a nonlinear, stiff, multi-parameter boundary-layer system—an ideal candidate for testing improved RK-type numerical integrators. Explicit stabilized and modified RK schemes provide a powerful balance between computational simplicity and enhanced stability, enabling larger timesteps without loss of accuracy. Recent numerical approaches involving boundary-layer flows over Riga plates [20–22] further reinforce the need for integrators that can handle strong electromagnetic forcing and porous-inertia effects under thermal–viscous coupling.

In this study, we develop a modified Runge–Kutta scheme incorporating stability-enhancement techniques inspired by stabilized RK theory [5–9, 23] and nonlinear convergence theory [10–12]. The method is analyzed for stability and convergence under the nonlinearities associated with Darcy–Forchheimer resistance, Eyring–Prandtl rheology, Riga plate electromagnetic forcing, and viscous dissipation. The numerical results show that the modified RK method significantly enlarges the allowable timestep relative to classical explicit RK while maintaining accuracy comparable to implicit schemes. This builds upon the previous works on stabilized RK methods [5–9], non-Newtonian Darcy–Forchheimer systems [13–19], and Riga-plate flows [20–22], integrating these strands into a unified computational framework.

The remainder of this paper is organized as follows: Section 2 presents the mathematical formulation and nondimensionalization. Section 3 describes the numerical method employed. In Section 4, we present and discuss the results. Finally, Section 5 gives concluding remarks.

Construction of Numerical Scheme: A three-stage computational scheme is going to be proposed for solving time dependent partial differential equations. The scheme is explicit in all three stages. The solution obtained in first stage will be utilized in second stage of scheme and similar solutions obtained from second stage will be utilized in third stage. The domain of the considered differential equation is denoted by $[0, L]$. This whole domain is divided into a equal subinterval of time $[0, t_f]$ is divided into equal small subintervals with length Δt. The scheme is constructed for following equation.

$$\frac{\partial g}{\partial t} = \alpha_1 \frac{\partial g}{\partial y} + \beta_1 \frac{\partial^2 g}{\partial y^2} + s(g) \tag{1}$$

Where s is linear or nonlinear function in g. The initial and boundary condition for Eq. (1) can be written as

$$\left.\begin{array}{c} g(0, y) = f_1(y) \\ g(t, 0) = f_2(t), and\ g(t, L) = f_3(t) \end{array}\right\} \tag{2}$$

Where α_1 and β_1 are constants and $f_j, j = 1,2,3$ are functions of t or some constants.
The first stage of the scheme for Eq. (1) is

$$\bar{g}_j^{n+1} = g_j^n e^{a_1 \Delta t} + \frac{(e^{a_1 \Delta t} - 1)}{a_1} \left\{ \left.\frac{\partial g}{\partial t}\right|_j^n - a_1 g_j^n \right\}. \tag{3}$$

Where subscript j is used for location of grid point and n represents point in time and a_1 is a free parameter. Stability region of these types of proposed schemes depends on value of this free parameter a_1.
This first stage (3) can be expressed as

$$\bar{g}_j^{n+1} = g_j^n + \frac{(e^{a_1 \Delta t} - 1)}{a_1} \left.\frac{\partial g}{\partial t}\right|_j^n, \tag{4}$$

where $\frac{(e^{a_1 \Delta t} - 1)}{a_1} \approx \Delta t + O(\Delta t^2)$.

So, this first stage of proposed scheme can be considered as modified form of existing Euler method
The second stage of the scheme is written as:

$$\bar{\bar{g}}_j^{n+1} = a g_j^n + b\bar{g}_j^{n+1} + \frac{1}{4}\Delta t \left.\frac{\partial \bar{g}}{\partial t}\right|_j^{n+1} \tag{5}$$

The third stage of the scheme for Eq. (1) takes the form

$$g_j^{n+1} = c g_j^n + d\bar{\bar{g}}_j^{n+1} + \frac{2}{3}\Delta t \left.\frac{\partial \bar{\bar{g}}}{\partial t}\right|_j^{n+1} \tag{6}$$

The unknown parameters a, b, c and d can be found later by matching the Taylor series expansion. Now combing the first stage Eq. (3) and second stage Eq. (5) of proposed scheme yields

$$\bar{\bar{g}}_j^{n+1} = (a+b)g_j^n + \left(\frac{b}{a_1}(e^{a_1\Delta t} - 1) + \frac{\Delta t}{4}\right)\left.\frac{\partial g}{\partial t}\right|_j^n + \frac{\Delta t}{4a_1}(e^{a_1\Delta t} - 1)\left.\frac{\partial^2 g}{\partial t^2}\right|_j^n \tag{7}$$

Now substituting Eq. (7) into Eq. (6) that yields the following equation:

$$g_j^{n+1} = c g_j^n + d\left[(a+b)g_j^n + \left\{\frac{b}{a_1}(e^{a_1\Delta t} - 1) + \frac{\Delta t}{4}\right\}\left.\frac{\partial g}{\partial t}\right|_j^n + \frac{\Delta t}{4a_1}(e^{a_1\Delta t} - 1)\left.\frac{\partial^2 g}{\partial t^2}\right|_j^n\right] + \frac{2}{3}\Delta t\left[(a+b)\left.\frac{\partial g}{\partial t}\right|_j^n + \left\{\frac{b}{a_1}(e^{a_1\Delta t} - 1) + \frac{\Delta t}{4}\right\}\left.\frac{\partial^2 g}{\partial t^2}\right|_j^n + \frac{\Delta t}{4a_1}(e^{a_1\Delta t} - 1)\left.\frac{\partial^3 g}{\partial t^3}\right|_j^n\right] \tag{8}$$

Expanding g_j^{n+1} using Taylor series expansion

$$g_j^{n+1} = g_j^n + \Delta t\left.\frac{\partial g}{\partial t}\right|_j^n + \frac{(\Delta t)^2}{2}\left.\frac{\partial^2 g}{\partial t^2}\right|_j^n + \frac{(\Delta t)^3}{6}\left.\frac{\partial^3 g}{\partial t^3}\right|_j^n + O((\Delta t)^4) \tag{9}$$

Using Eq. (9) into Eq. (8) that results in

$$g_j^n + \Delta t\left.\frac{\partial g}{\partial t}\right|_j^n + \frac{(\Delta t)^2}{2}\left.\frac{\partial^2 g}{\partial t^2}\right|_j^n + \frac{(\Delta t)^3}{6}\left.\frac{\partial^3 g}{\partial t^3}\right|_j^n = [c + d(a+b)]g_j^n + \left[\frac{bd}{a_1}(e^{a_1\Delta t} - 1) + \frac{\mathrm{d}\Delta t}{4} + \frac{2}{3}\Delta t(a+b)\right]\left.\frac{\partial g}{\partial t}\right|_j^n + \left[\frac{\mathrm{d}\Delta t}{4a_1}(e^{a_1\Delta t} - 1) + \frac{2}{3}\Delta t\left(\frac{b}{a_1}(e^{a_1\Delta t} - 1) + \frac{1}{4}\Delta t\right)\right]\left.\frac{\partial^2 g}{\partial t^2}\right|_j^n + \frac{(\Delta t)^2}{6a_1}(e^{a_1\Delta t} - 1)\left.\frac{\partial^3 g}{\partial t^3}\right|_j^n \tag{10}$$

Equating the coefficients of $g_j^n, \left.\frac{\partial g}{\partial t}\right|_j^n, \left.\frac{\partial^2 g}{\partial t^2}\right|_j^n$ and $\left.\frac{\partial^3 g}{\partial t^3}\right|_j^n$ on both sides of Eq. (10), it gives

$$\left.\begin{aligned} 1 &= c + d(a+b) \\ \Delta t &= \frac{bd}{a_1}(e^{a_1\Delta t} - 1) + \frac{\mathrm{d}\Delta t}{4} + \frac{2}{3}\Delta t(a+b) \\ \frac{(\Delta t)^2}{2} &= \frac{\mathrm{d}\Delta t}{4a_1}(e^{a_1\Delta t} - 1) + \frac{2}{3}\Delta t\left(\frac{b}{a_1}(e^{a_1\Delta t} - 1) + \frac{1}{4}\Delta t\right) \\ \frac{(\Delta t)^3}{6} &= \frac{(\Delta t)^2}{6a_1}(e^{a_1\Delta t} - 1) \end{aligned}\right\} \tag{11}$$

Applying condition of $a + b = 1$ and solving the linear system of Eq. (11) gives the values of a, b, c and d as follows

$$\left.\begin{aligned} a &= \frac{3\Delta t - \sqrt{\Delta t(9\Delta t - 8\gamma(\Delta t))}}{8\gamma(\Delta t)} - \frac{\Delta t - 2\gamma(\Delta t)}{2\gamma(\Delta t)} \\ b &= \frac{\Delta t + \sqrt{\Delta t(9\Delta t - 8\gamma(\Delta t))}}{8\gamma(\Delta t)} - \frac{\Delta t - 2\gamma(\Delta t)}{2\gamma(\Delta t)} \\ c &= \frac{\gamma(\Delta t) - \Delta t}{\gamma(\Delta t)} - \frac{\sqrt{\Delta t(9\Delta t - 8\gamma(\Delta t))}}{3\gamma(\Delta t)} \\ d &= \frac{6\Delta t - \sqrt{\Delta t(9\Delta t - 8\gamma(\Delta t))}}{6\gamma(\Delta t)} \end{aligned}\right\} \tag{12}$$

where $\gamma(\Delta t) = \frac{e^{a_1\Delta t - 1}}{a_1}$.

The proposed scheme is three stages that can be used for time discretization of partial differential equations. To discretize space dependent terms a compact scheme is employed. The proposed scheme for Eq. (1) with compact spatial discretization [24] takes the form:

$$\bar{g}_j^{n+1} = g_j^n e^{1.5\Delta t} + \frac{(e^{a_1\Delta t}-1)}{a_1}\left\{\alpha_1\zeta_1\, g_j^n + \beta_1\zeta_2\, g_j^n - \frac{3}{2}g_j^n\right\} \tag{13}$$

$$\bar{\bar{g}}_j^{n+1} = a g_j^n + b\bar{g}_j^{n+1} + \frac{1}{4}\Delta t\left\{\alpha_1\zeta_1\, \bar{g}_j^{n+1} + \beta_1\zeta_2\, \bar{g}_j^{n+1}\right\} \tag{14}$$

$$g_j^{n+1} = c g_j^n + d\bar{\bar{g}}_j^{n+1} + \frac{2}{3}\Delta t\left\{\alpha_1\zeta_1\, \bar{\bar{g}}_j^{n+1} + \beta_1\zeta_2\, \bar{\bar{g}}_j^{n+1}\right\} \tag{15}$$

Where $\zeta_1 = A_1^{-1}B_1$ & $\zeta_2 = A_2^{-1}B_2$.
Where A_l, B_l for $l = 1,2$ are matrices constructed from the coefficients of left and right hand sides of the following equations

$$\gamma_1 \frac{\partial g}{\partial y}\bigg|_{j-1}^{n} + \frac{\partial g}{\partial y}\bigg|_{j}^{n} + \gamma_1 \frac{\partial g}{\partial y}\bigg|_{j+1}^{n} = b_0 \frac{(g_{j+1}^n - g_{j-1}^n)}{2\Delta y} + b_1 \frac{(g_{j+2}^n - g_{j-2}^n)}{4\Delta y} \tag{16}$$

$$\gamma_2 \frac{\partial^2 g}{\partial y^2}\bigg|_{j-1}^{n} + \frac{\partial^2 g}{\partial y^2}\bigg|_{j}^{n} + \gamma_2 \frac{\partial^2 g}{\partial y^2}\bigg|_{j+1}^{n} = b_2 \frac{(g_{j+1}^n - 2g_j^n + g_{j-1}^n)}{(\Delta y)^2} + b_3 \frac{(g_{j+2}^n - 2g_j^n + g_{j-2}^n)}{4(\Delta y)^2} \tag{17}$$

Where $b_0 = \frac{\gamma_1+2}{3}, b_1 = \frac{1-4\gamma_1}{3}, b_2 = \frac{4(1-\gamma_2)}{3}, b_3 = \frac{10\gamma_2-1}{3}$.

Stability Analysis: One of the tasks in finite differences is to check their stability region. There exists more than one stability analysis for finding stability conditions for finite difference schemes. Among existing stability analysis Fourier series analysis or Von Neumann stability analysis is a stability procedure that can be used to find stability conditions of finite difference schemes applied to linear partial differential equation. The analysis is started by transforming a given difference equation into a trigonometric equation. For this case the transformations can be expressed as:

$$A_1 e^{ij\psi} = e^{ij\psi}\left(\gamma_1 e^{i\psi} + 1 + \gamma_1 e^{-i\psi}\right) \tag{18}$$

$$B_1 e^{ij\psi} = \frac{b_\circ e^{(j+1)i\psi}}{2\Delta y} - \frac{b_\circ e^{(j-1)i\psi}}{2\Delta y} + \frac{b_1 e^{(j+2)i\psi}}{4\Delta y} - \frac{b_1 e^{(j-2)i\psi}}{4\Delta y} \tag{19}$$

$$A_2 e^{ij\psi} = e^{ij\psi}\left(\gamma_2 e^{2i\psi} + 1 + \gamma_2 e^{-2i\psi}\right) \tag{20}$$

$$B_2 e^{ij\psi} = \frac{b_2 e^{(j+1)i\psi}}{(\Delta y)^2} - \frac{2b_2 e^{ji\psi}}{(\Delta y)^2} + \frac{b_2 e^{(j-1)i\psi}}{(\Delta y)^2} + \frac{b_3 e^{(j+2)i\psi}}{4(\Delta y)^2} - \frac{2b_3 e^{ji\psi}}{4(\Delta y)^2} + \frac{b_3 e^{(j-2)i\psi}}{4(\Delta y)^2} \tag{21}$$

Where $i = \sqrt{-1}$.
Applying transformations (19) - (21) into first stage of the scheme (13) gives

$$\bar{g}_j^{n+1} = g_i^n e^{1.5\Delta t} + \frac{(e^{1.5\Delta t}-1)}{1.5}\left\{\begin{array}{c}\alpha_1\left(\frac{2b_0 i\sin\psi + c_1 i\sin 2\psi}{2\Delta y(2\gamma_1\cos\psi+1)}\right) + \\ \beta_1\left(\frac{4b_2(\cos\psi-1)+b_3(\cos 2\psi-1)}{2(\Delta y)^2(2\gamma_2\cos\psi-1)}\right) - \frac{3}{2}\end{array}\right\} g_j^n \tag{22}$$

Re-write Eq. (22) as

$$\bar{g}_j^{n+1} = (c_1 + ic_2)g_j^n \tag{23}$$

Where $\mu_{c_1} = e^{1.5\Delta t} + \frac{(e^{1.5\Delta t}-1)}{1.5}\left\{\beta_1\left(\frac{4b_2(\cos\psi-1)+b_3(\cos 2\psi-1)}{2(\Delta y)^2(2\gamma_2\cos\psi-1)}\right) - \frac{3}{2}\right\}$, and $\mu_{c_2} = \frac{(e^{1.5\Delta t}-1)}{1.5}\left\{\alpha_1\left(\frac{2b_0 i\sin\psi + c_1 i\sin 2\psi}{2\Delta y(2\gamma_1\cos\psi+1)}\right)\right\}$

Substituting transformations (19)-(21) into the second stage of the scheme (14) gives.

$$\bar{\bar{g}}_j^{n+1} = a g_j^n + b\bar{g}_j^{n+1} + \frac{1}{4}\Delta t\left\{\alpha_1\left(\frac{2b_0 i\sin\psi + c_1 i\sin 2\psi}{2\Delta y(2\gamma_1\cos\psi+1)}\right) + \beta_1\left(\frac{4b_2(\cos\psi-1)+b_3(\cos 2\psi-1)}{2(\Delta y)^2(2\gamma_2\cos\psi-1)}\right)\right\}\bar{g}_j^{n+1} \tag{24}$$

Eq. (24) can be written as

$$\bar{\bar{g}}_j^{n+1} = \mu_1 g_j^n \tag{25}$$

where $\mu_1 = \mu_{c_5} + i\mu_{c_6}$, $\mu_{c_5} = a + \mu_{c_1}\mu_{c_3} - \mu_{c_2}\mu_{c_4}$ and $\mu_{c_6} = \mu_{c_1}\mu_{c_4} + \mu_{c_2}\mu_{c_3}$

and $\mu_{c_3} = b + \frac{1}{4}\Delta t\left\{\beta_1\left(\frac{4b_2(\cos\psi-1)+b_3(\cos 2\psi-1)}{2(\Delta y)^2(2\gamma_2\cos\psi-1)}\right)\right\}$, & $\mu_{c_4} = \frac{1}{4}\Delta t\left\{\alpha_1\left(\frac{2b_0 i\sin\psi + c_1 i\sin 2\psi}{2\Delta y(2\gamma_1\cos\psi+1)}\right)\right\}$

By using transformations (19)-(21) into third stage of the scheme (15) gives

$$g_j^{n+1} = \mu_2 g_j^n \tag{26}$$

Where $\mu_2 = \mu_{c_9} + i\mu_{c_{10}}, \mu_{c_9} = c + \mu_{c_7}\mu_{c_5} - \mu_{c_6}\mu_{c_8}$ and $\mu_{c_{10}} = \mu_{c_6}\mu_{c_7} + \mu_{c_5}\mu_{c_8}$
and $\mu_{c_7} = c + \frac{2}{3}\Delta t\left\{\beta_1\left(\frac{4b_2(cos\psi-1)+b_3(cos2\psi-1)}{2(\Delta y)^2(2\gamma_2\cos\psi-1)}\right)\right\}$
$\mu_{c_8} = \frac{2}{3}\Delta t\alpha_1\left(\frac{2b_0 isin\psi+c_1 isin2\psi}{2\Delta y(2\gamma_1\cos\psi+1)}\right)$.

The amplification factor can be written as

$$\left|\frac{g_j^{n+1}}{g_j^n}\right|^2 = \mu_{c_9}^2 + \mu_{c_{10}}^2 \tag{27}$$

So, the scheme will be stable if it satisfies

$$\mu_{c_9}^2 + \mu_{c_{10}}^2 \leq 1 \tag{28}$$

For the case when $\alpha_1 = 0$, stability condition can be expressed as

$$|G| < 1 \tag{29}$$

where $G = \frac{d^3\Gamma^3\gamma(\Delta t)+d^2\Gamma^2(\Delta t+2\gamma(\Delta t))+d\,\Gamma(5\Delta t+\gamma(\Delta t))+6\Delta t}{6\Delta t}$, $\Gamma = \frac{2b_2(cos(\psi)-1)+0.5b_2(cos(2\psi)-1)}{2\gamma_2\cos\psi+1}$,
and $d = \beta_1\frac{\Delta t}{\Delta y^2}$, $\gamma(\Delta t) = \frac{e^{a_1\Delta t}-1}{a_1}$.

Fig. 1 shows the comparison of stability region G along diffusion number d for different values of time step sizes and free parameter a_1. Amplification factor G is found by applying first stage of proposed scheme and second and third stage of existing third order Runge-Kutta method. Stability region of this tye of scheme depend on choice of free parameter a_1 and choice of time step size Δt.

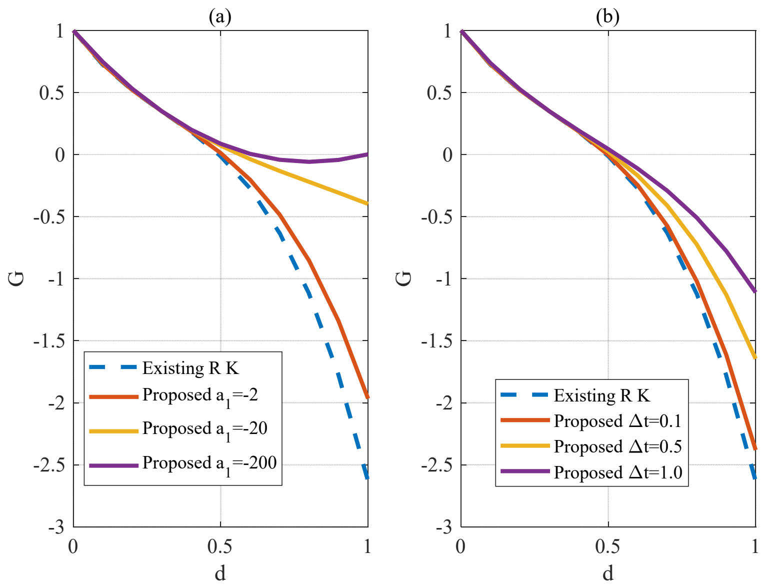

Figure 1. Comprison of stability regions of proposed and existing Runge-Kutta methods (a) $\Delta t = 0.3, \gamma_2 = -0.3$ (b) $\gamma_2 = -0.3\,, a_1 = -2$

The stability of the proposed scheme is provided for scalar partial differential equations. Now the convergence of the proposed scheme for system of convection diffusion equation is provided.
For doing so consider the vector matrix equation of the form

$$\boldsymbol{v_t} = C_1\boldsymbol{v_y} + C_2\boldsymbol{v_{yy}} + C_3\boldsymbol{v} \tag{30}$$

Where v is a vector and C_1, C_2 and C_3 are matrices. Eq. (30) is discretized by the proposed scheme as

$$\overline{\boldsymbol{v}}_j^{n+1} = \boldsymbol{v}_j^n e^{1.5\Delta t} + \frac{(e^{a_1\Delta t}-1)}{a_1}\{C_1\zeta_1 + C_2\zeta_2 + C_3\boldsymbol{v}_j^n - a_1\}\boldsymbol{v}_j^n \tag{31}$$

$$\bar{\bar{\boldsymbol{v}}}_j^{n+1} = a\boldsymbol{v}_j^n + \left[b + \frac{1}{4}\Delta t\{C_1\zeta_1 + C_2\zeta_2 + C_3\}\right]\bar{\boldsymbol{v}}_j^{n+1} \tag{32}$$

$$\boldsymbol{v}_j^{n+1} = c\boldsymbol{v}_j^n + \left[d + \frac{2}{3}\Delta t\{C_1\zeta_1 + C_2\zeta_2 + C_3\}\right]\bar{\bar{\boldsymbol{v}}}_j^{n+1} \tag{33}$$

Theorem: The proposed scheme (31)-(33) converges conditionally for vectored matrix Eq. (30).
Proof: In order to proof this Theorem consider the error equation for Eq. (27) as:

$$\bar{\boldsymbol{\varsigma}}_j^{n+1} = \boldsymbol{\varsigma}_j^n e^{1.5\Delta t} + \frac{(e^{a_1\Delta t}-1)}{a_1}\left\{C_1\zeta_1\,\boldsymbol{\varsigma}_j^n + C_2\zeta_2\,\boldsymbol{\varsigma}_j^n + C_3\boldsymbol{\varsigma}_j^n - a_1\boldsymbol{\varsigma}_j^n\right\} \tag{34}$$

$$\bar{\bar{\boldsymbol{\varsigma}}}_j^{n+1} = a\boldsymbol{\varsigma}_j^n + b\bar{\boldsymbol{\varsigma}}_j^{n+1} + \frac{1}{4}\Delta t\left\{C_1\zeta_1\,\bar{\boldsymbol{\varsigma}}_j^{n+1} + C_2\zeta_2\,\bar{\boldsymbol{\varsigma}}_j^{n+1} + C_3\bar{\boldsymbol{\varsigma}}_j^{n+1}\right\} \tag{35}$$

$$\boldsymbol{\varsigma}_j^{n+1} = c\boldsymbol{\varsigma}_j^n + d\bar{\bar{\boldsymbol{\varsigma}}}_j^{n+1} + \frac{2}{3}\Delta t\left\{C_1\zeta_1\,\bar{\bar{\boldsymbol{\varsigma}}}_j^{n+1} + C_2\zeta_2\,\bar{\bar{\boldsymbol{\varsigma}}}_j^{n+1} + C_3\bar{\bar{\boldsymbol{\varsigma}}}_j^{n+1}\right\} \tag{36}$$

Applying a norm $\|\cdot\|_\infty$ on first stage of Eq. (34) in the form

$$\bar{\varsigma}^{n+1} \le \varsigma^n e^{1.5\Delta t} + \frac{(e^{a_1\Delta t}-1)}{a_1}\{\|C_1\zeta_1\|_\infty + \|C_2\zeta_2\|_\infty + \|C_3\|_\infty + a_1\}\varsigma^n \tag{37}$$

Inequality (37) can be written as

$$\bar{\varsigma}^{n+1} \le \beta_2\varsigma^n \tag{38}$$

Where $\beta_2 = e^{a_1\Delta t} + \frac{(e^{a_1\Delta t}-1)}{a_1}\{\|C_1\zeta_1\|_\infty + \|C_2\zeta_2\|_\infty + \|C_3\|_\infty + a_1\}$.
Applying norm $\|\cdot\|_\infty$ on Eq. (35) as yields

$$\bar{\bar{\varsigma}}^{n+1} \le a\varsigma^n + b\bar{\varsigma}^{n+1} + \frac{1}{4}\Delta t\{\|C_1\zeta_1\|_\infty + \|C_2\zeta_2\|_\infty + \|C_3\|_\infty\}\bar{\varsigma}^{n+1} = a\varsigma^n + \beta_3\bar{\varsigma}^{n+1} \tag{39}$$

where $\beta_3 = b + \frac{1}{4}\Delta t\{\|C_1\zeta_1\|_\infty + \|C_2\zeta_2\|_\infty + \|C_3\|_\infty\}$.
Inequality (39) can be re written as

$$\bar{\bar{\varsigma}}^{n+1} \le a\varsigma^n + \beta_3\beta_2\varsigma^n = \beta_4\varsigma^n \tag{40}$$

where $\beta_4 = a + \beta_2\beta_3$.
Similarly by applying a norm $\|\cdot\|_\infty$ to third error equation of the scheme (36), it gives

$$\varsigma^{n+1} \le c\varsigma^n + d\bar{\bar{\varsigma}}^{n+1} + \frac{2}{3}\Delta t\{\|C_1\zeta_1\|_\infty + \|C_2\zeta_2\|_\infty + \|C_3\|_\infty\}\bar{\bar{\varsigma}}^{n+1} \tag{41}$$

Inequality (41) can be re-written as

$$\varsigma^{n+1} \le c\varsigma^n + \beta_5\bar{\bar{\varsigma}}^{n+1} + P\big(O((\Delta t)^3, (\Delta y)^6)\big) \tag{42}$$

Substituting inequality (40) into inequality (42), it takes the form

$$\varsigma^{n+1} \le c\varsigma^n + \beta_5\beta_4\varsigma^n + P\big(O((\Delta t)^3, (\Delta y)^6)\big) = \beta_6\varsigma^n + P\big(O((\Delta t)^3, (\Delta y)^6)\big) \tag{43}$$

where $\beta_6 = c + \beta_4\beta_5$.
Let $n = 0$ in inequality (43), it yields

$$\varsigma^1 \le \beta_6\varsigma^0 + P\big(O((\Delta t)^3, (\Delta y)^6)\big) \tag{44}$$

Since $\varsigma^0 = 0$ so inequality (44) takes the form

$$\varsigma^1 \le P(0((\Delta t)^3, (\Delta y)^6)) \tag{45}$$

Now let $n = 1$ in inequality (43) it yields

$$\varsigma^2 \le \beta_6\varsigma^1 + P(0((\Delta t)^3, (\Delta y)^6)) \tag{46}$$

Using inequality (45) in (46) it results in

$$\varsigma^2 \le (1 + \beta_6)P(0((\Delta t)^3, (\Delta y)^6)) \tag{47}$$

If this is continuous then for finite n

$$\varsigma^n \le (1+\beta_6+\cdots+\beta_6^{n-1})P(0((\Delta t)^3,(\Delta y)^6)) = \left(\frac{1-\beta_6^n}{1-\beta_6}\right)P(0((\Delta t)^3,(\Delta y)^6)) \tag{48}$$

By taking limit as $n\to\infty$ in (44) the infinite geometric series $\ldots+\beta_6^n+\cdots+\beta_6+1$ will converge if $|\beta_6|<1$.

Mathematical Model: We consider the unsteady, one-dimensional incompressible flow of an Eyring–Prandtl fluid through a porous medium over a Riga plate, with heat and mass transfer, viscous dissipation, and mixed convection. The streamwise velocity $u(t,y)$ varies only in the wall-normal coordinate y^*; the momentum balance couples temporal acceleration to the divergence of the Eyring–Prandtl shear stress the streamwise Lorentz body force from the Riga plate and porous resistance expressed by linear Darcy drag $-\frac{\mu}{K}u^*$ and nonlinear Forchheimer drag $-\frac{\rho F}{\sqrt{K}}u^{*2}$. Mixed convection is modeled under the Boussinesq approximation by adding buoyancy forces $g\beta_T(T-T_\infty)+g\beta_C(C-C_\infty)$ in the momentum equation, so thermal and solutal buoyancy couple the momentum, energy and species fields. Heat transfer is described by the unsteady energy equation with thermal diffusion and viscous dissipation arising from the Eyring–Prandtl stress, while mass transfer follows the unsteady species diffusion equation (with optional reaction/source terms). The wall at $y^*=0$ is maintained at prescribed velocity $u^*(t,0)=u_w+L_s\frac{\partial u^*}{\partial y^*}$, convective boundary temperature $-k\frac{\partial T(t,0)}{\partial y^*}=h_f(T(t,0)-T_w)$ and concentration $C(t,0)=C_w$; far from the plate $u^*\to 0, T\to T_\infty, C\to C_\infty$ as $y^*\to\infty$. Initially the fluid is quiescent and uniform in temperature and concentration. The objective is to determine the transient distributions $u^*(t,y),T(t,y),C(t,y)$ under the combined influences of Eyring–Prandtl rheology, Riga electromagnetic forcing, Darcy–Forchheimer porous resistance, thermal and solutal buoyancy (mixed convection), molecular diffusion, and viscous dissipation. The governing equations can be written as:

$$\rho\frac{\partial u^*}{\partial t^*} = \frac{\bar\beta}{\bar C}\left(\frac{\frac{\partial^2 u^*}{\partial y^{*2}}}{\sqrt{1+\left(\frac{1\partial u^*}{\bar C\partial y^*}\right)^2}}\right) - \frac{\mu}{K}u - \frac{\rho C_f}{\sqrt{K}}u^{*2} + g\beta_T(T-T_\infty) + \beta_C(C-C_\infty) + \frac{\pi j_\circ M_\circ}{8\rho}e^{-\left(\frac{\pi}{a_1}\right)y^*} \tag{49}$$

$$\frac{\partial T}{\partial t^*} = \bar\alpha\frac{\partial^2 T}{\partial y^{*2}} + \frac{\bar\beta}{\rho C_p}\sinh^{-1}\left(\frac{1}{\bar C}\frac{\partial u^*}{\partial y^*}\right)\frac{\partial u^*}{\partial y^*} \tag{50}$$

$$\frac{\partial C}{\partial t^*} = D\frac{\partial^2 C}{\partial y^{*2}} - k_1(C-C_\infty) \tag{51}$$

Subject to initial and boundary conditions

$$\left.\begin{array}{c} u^*(0,y^*)=0, T(0,y^*)=0, C(0,y^*)=0 \\ u^*(t^*,0)=u_w+L_s\left.\frac{\partial u^*}{\partial y^*}\right|_{y^*=0}, -k\left.\frac{\partial T}{\partial y^*}\right|_{y^*=0} = h_f(T(t^*,0)-T_w), C(t^*,0)=C_w \\ u^*(t^*,y^*\to\infty)\to 0, T(t^*,y^*\to\infty)\to 0, C(t^*,y^*\to\infty)\to 0 \end{array}\right\} \tag{52}$$

Where u^* is the horizontal component of velocity, T is the temperature and C is concentration, β_T and β_C are thermal and solutan expansion, $\bar\beta$ is the stress parameter, $\bar C$ is the rate parameter, $j_\circ$ is the current density, $M_\circ$is a magnetic field strength, a_1 width of electrodes, g is gravity, K is the permeability of the porous medium, C_f is dimensionless constant representing inertial drag in the porous medium, ρ is density, $\bar\alpha$ is thermal diffusivity, D is mass diffusivity and k_1 is dimensional reaction rate parameter, h_f is heat transfer coefficient and k is thermal conductivity

Using the transformations

$$\left. y=\frac{y^*}{L}, u=\frac{u^*}{u_w}, t=\frac{u_w t^*}{L}, \theta=\frac{T-T_\infty}{T_w-T_\infty}, \phi=\frac{C-C_\infty}{C_w-C_\infty}\right\} \tag{53}$$

The governing equations (49)-(52) are reduced to following dimensionless partial differential equations

$$\frac{\partial u}{\partial t} = \frac{1}{R_e}\left(\frac{u_{yy}}{\sqrt{1+S^2u_y^2}}\right) - \frac{1}{R_eD_a}u - F_r u^2 + \frac{G_{\gamma_L}}{R_e^2}\theta + \frac{G_{\gamma_C}}{R_e^2}\phi + e^{-\lambda y} \tag{54}$$

$$\frac{\partial\theta}{\partial t} = \frac{1}{P_rR_e}\frac{\partial^2\theta}{\partial y^2} + \frac{E_c}{R_eS}\sinh^{-1}(Su_y) \tag{55}$$

$$\frac{\partial\phi}{\partial t} = \frac{1}{R_eS_c}\frac{\partial^2\phi}{\partial y^2} - \gamma\phi \tag{56}$$

and the dimensionless initial and boundary conditions take the form

$$\left.\begin{array}{c} u(0,y)=0,\theta(0,y)=0,\phi(0,y)=0 \\ u(t,0)=1+\Lambda\left.\frac{\partial u}{\partial y}\right|_{y=0},\left.\frac{\partial\theta}{\partial y}\right|_{y=0}=B_i(1-\theta(t,0)),\phi(t,0)=1 \\ u(t,y\to\infty)\to 0,\theta(t,y\to\infty)\to 0,\phi(t,y\to\infty)\to 0 \end{array}\right\} \tag{57}$$

Where D_a is Darcy number, F_r is Forchheimer number, S is Eyring (shear) number, R_e is Reynolds number, M is dimensionless electromagnetic Riga parameter, λ is dimensionless decay rate of Lorentz force in the y- direction, G_{γ_L} and G_{γ_C} are respectively thermal and solutal Grashof number, P_r is Prandtl number, E_c is Eckert number, S_c is Schnidt number, γ is dimensionless reaction rate parameter, and Λ is velocity slip and B_i is Boit number which are defined as:

$D_a=\frac{K}{L^2},F_r=\frac{C_fL}{\sqrt{K}},S=\frac{u_w}{\bar{C}L},R_e=\frac{u_wL}{\nu}=\frac{\rho u_wL\bar{C}}{\bar{\beta}},M=\frac{\pi j_\circ M_\circ L}{8\rho u_w^2},\lambda=\frac{\pi}{a_1}L,G_{\gamma_L}=\frac{g\beta_T(T_w-T_\infty)}{\nu^2},G_{\gamma_C}=\frac{g\beta_C(C_w-C_\infty)}{\nu^2},P_r=\frac{\nu}{\bar{\alpha}},E_c=\frac{u_w^2}{C_p(T_w-T_\infty)},S_c=\frac{\nu}{D},\gamma=\frac{k_1L}{u_w},\Lambda=\frac{L_s}{L},B_i=\frac{h_\lambda}{Lk}$

The dimensionless skin friction coefficients, local Nusselt and local Sherwood number are written as:

$$\left.\begin{array}{c} \bar{C_f}=\frac{1}{R_eS}\sinh^{-1}\left(Su_y\big|_{y=0}\right) \\ N_{u_L}=-\left.\frac{\partial\theta}{\partial y}\right|_{y=0} \\ S_{h_L}=-\left.\frac{\partial\phi}{\partial y}\right|_{y=0} \end{array}\right\} \tag{58}$$

The discretization of Eq. (54) using the proposed scheme it takes the form:

$$\bar{u}_j^{n+1}=u_j^ne^{a_1\Delta t}+\frac{\left(e^{a_1\Delta t}-1\right)}{a_1}\left\{\frac{\frac{1}{R_e}\left(A_2^{-1}B_2\,u_j^n\right)}{\sqrt{1+S^2\left(A_1^{-1}B_1\,u_j^n\right)^2}}-\frac{1}{R_eD_a}\,u_j^n-F_r\left(u_j^n\right)^2+\frac{G_{\gamma_L}}{R_e^2}\,\theta_j^n+\frac{G_{\gamma_C}}{R_e^2}\,\phi_j^n+Me^{-\lambda y_j}-a_1u_j^n\right\} \tag{59}$$

$$\bar{\bar{u}}_j^{n+1}=au_j^n+b\bar{u}_j^{n+1}+\frac{1}{4}\Delta t\left\{\frac{\frac{1}{R_e}\left(A_2^{-1}B_2\,\bar{u}_j^{n+1}\right)}{\sqrt{1+S^2\left(A_1^{-1}B_1\,\bar{u}_j^{n+1}\right)^2}}-\frac{1}{R_eD_a}\,\bar{u}_j^{n+1}-F_r\left(\bar{u}_j^{n+1}\right)^2+\frac{G_{\gamma_L}}{R_e^2}\,\bar{\theta}_j^{n+1}+\frac{G_{\gamma_C}}{R_e^2}\,\bar{\phi}_j^{n+1}+Me^{-\lambda y_j}\right\} \tag{60}$$

$$u_j^{n+1}=cu_j^n+d\bar{\bar{u}}_j^{n+1}+\frac{2}{3}\Delta t\left\{\frac{\frac{1}{R_e}\left(A_2^{-1}B_2\,\bar{\bar{u}}_j^{n+1}\right)}{\sqrt{1+S^2\left(A_1^{-1}B_1\,\bar{\bar{u}}_j^{n+1}\right)^2}}-\frac{1}{R_eD_a}\,\bar{\bar{u}}_j^{n+1}-F_r\left(\bar{\bar{u}}_j^{n+1}\right)^2+\frac{G_{\gamma_L}}{R_e^2}\,\bar{\bar{\theta}}_j^{n+1}+\frac{G_{\gamma_C}}{R_e^2}\,\bar{\bar{\phi}}_j^{n+1}+Me^{-\lambda y_j}\right\} \tag{61}$$

RESULTS AND DISCUSSION

A third-order accurate time-stepping scheme is developed for the numerical solution of partial differential equations. The method is specifically designed for discretizing only the time-dependent term of the governing equation, and its accuracy is confirmed through its construction, where the third-order time derivative naturally cancels in the Taylor series expansion. For the spatial discretization, a compact high-order finite-difference scheme is employed, providing sixth-order accuracy in space. The overall scheme is conditionally stable, implying that the time step, spatial step, and the physical parameters appearing in the governing equation must satisfy a prescribed stability condition. When these restrictions are met, the numerical solution remains stable; otherwise, instability is expected. A notable benefit of using an explicit scheme is that it avoids the need for linearization, enabling direct treatment of nonlinear partial differential equations without any iterative procedure for convergence.

The influence of Eyring parameter on velocity profile is shown in Fig. 2. The velocity profile declines by raising Eyring number. Increasing the Eyring number means the fluid resists deformation more at low shear rates. Since most of the velocity in internal flows depends on the balance between pressure gradient and viscous resistance, this increased resistance lowers the velocity everywhere**.** The effect of Darcy number on velocity profile is depicted in Fig. 3. The velocity profile increases by growing Darcy number. Small Darcy number produces very low permeability and so porous medium strongly resists the flow. Large Darcy number gives high permeability and this leads to porous medium offers little resistance. Thus, increasing Darcy number reduces the Darcy resistance term in the momentum equation.

The effect of Forchheimer number on velocity profile is shown in Fig. 4. The velocity profile declines by growing Forchheimer number. Darcy drag (linear) dominates at low speeds. When velocity increases, inertial forces inside the porous medium become important. The Forchheimer term grows faster than velocity (proportional to u^2). Increasing the Forchheimer parameter amplifies this additional nonlinear drag, so the flow slows down. The velocity slip parameter on velocity profile is shown in Fig. 5. Velocity profile decays by enhancing velocity slip parameter. Increasing the

Forchheimer parameter enhances the nonlinear inertial drag inside the porous medium. This additional resistance reduces the fluid velocity, causing the velocity profile to decline even under slip-flow conditions for an Eyring–Prandtl fluid. Fig. 6 deliberates the effect of Eckert number on temperature profile. Temperature profile grows by enhancing Eckert number. Increasing the Eckert number enhances viscous dissipation, producing additional internal heat, which raises the temperature profile. The influence of reaction rate parameter on concentration profile is shown in Fig. 7.

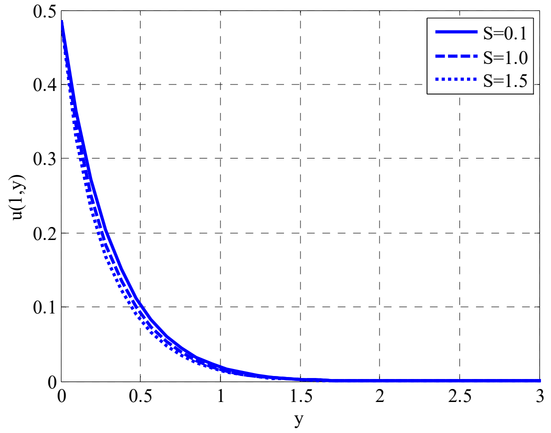

Figure 2. Effect of Eyring number on velocity profile using $Da = 0.1, Fr = 0.1, M = 0.1, \lambda = 3, \Lambda = 0.1, Re = 5, Gr_T = 0.1, Gr_C = 0.1, Ec = 5, Pr = 3, Sc = 3, \gamma = 0.9, Bi = 0.1$

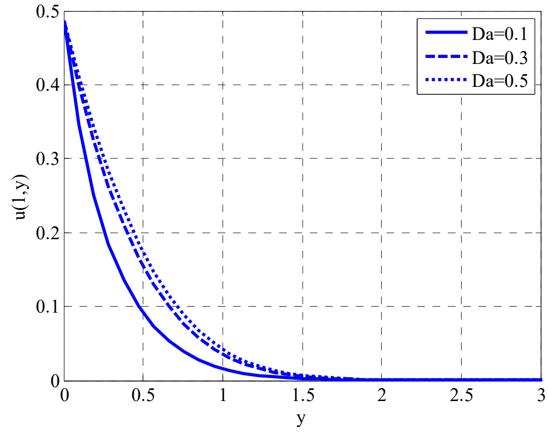

Figure 3. Effect of Darcy number on velocity profile using $S = 1, Fr = 0.1, M = 0.1, \lambda = 3, \Lambda = 0.1, Re = 5, Gr_T = 0.1, Gr_C = 0.1, Ec = 5, Pr = 3, Sc = 3, \gamma = 0.9, Bi = 0.1$

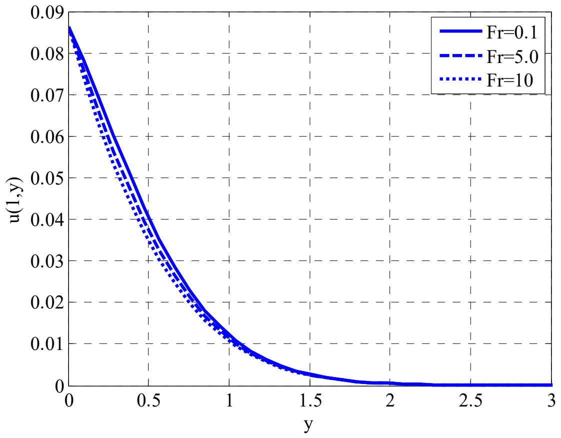

Figure 4. Effect of Forchheimer number on velocity profile using $S = 1, Da = 0.3, M = 0.1, \lambda = 3, \Lambda = 1, Re = 5, Gr_T = 0.1, Gr_C = 0.1, Ec = 5, Pr = 3, Sc = 3, \gamma = 0.9, Bi = 5$

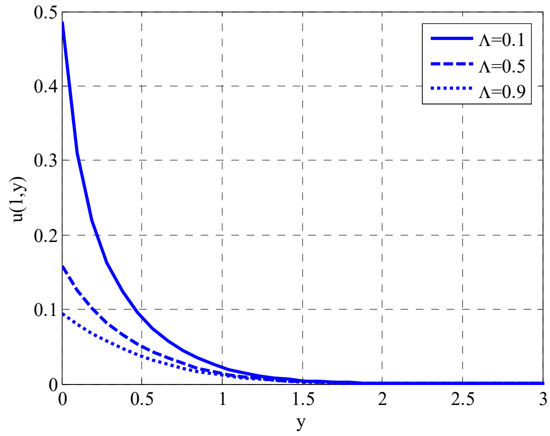

Figure 5. Effect of velocity slip parameter on velocity profile using $S = 1, Da = 0.3, M = 0.1, \lambda = 3, \mathrm{Fr} = 10, Re = 5, Gr_T = 0.1, Gr_C = 0.1, Ec = 5, Pr = 3, Sc = 3, \gamma = 0.9, Bi = 5$

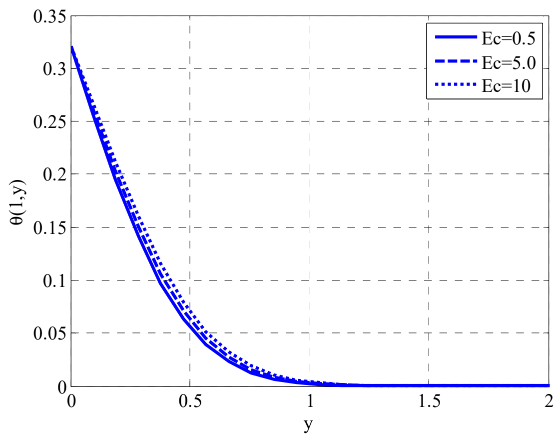

Figure 6. Effect of Eckert number on temperature profile using $S = 1, Da = 0.3, M = 0.1, \lambda = 3, \mathrm{Fr} = 10, Re = 5, Gr_T = 0.1, Gr_C = 0.1, \Lambda = 0.9, Pr = 3, Sc = 3, \gamma = 0.9, Bi = 5$

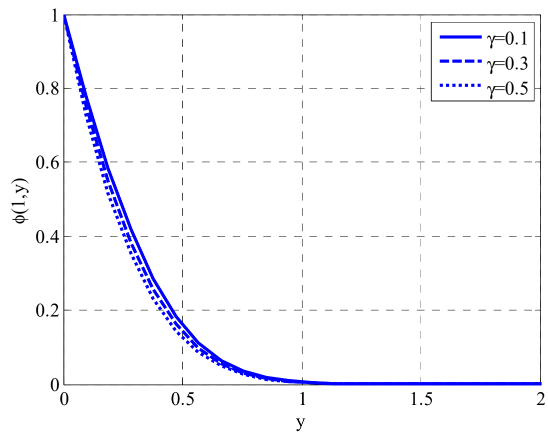

Figure 7. Effect of reaction rate parameter on concentration profile using $S = 1, Da = 0.3, M = 0.1, \lambda = 3, \mathrm{Fr} = 10, Re = 5, Gr_T = 0.1, Gr_C = 0.1, \Lambda = 0.9, Pr = 3, Sc = 3, Ec = 10, Bi = 5$

Concentration profile declines by enhancing reaction rate parameter. Increasing the reaction-rate parameter enhances species consumption, thereby reducing concentration and lowering the concentration profile. For the oscillatory motion of the Riga plate, the influence of velocity slip on the skin-friction coefficient is illustrated in Fig. 8. The results indicate an oscillatory pattern, where negative values of the skin-friction coefficient signify that the fluid near the wall momentarily moves in the direction opposite to the mean flow. The effect of the Biot number on the local Nusselt number is presented in Fig. 9, showing that heat transfer at the wall strengthens as the Biot number increases. A larger Biot number corresponds to a steeper temperature gradient at the surface, resulting in more efficient heat exchange between the plate and the fluid, and consequently a higher local Nusselt number. The oscillatory nature of the Nusselt number becomes more pronounced at elevated Eckert numbers, indicating that as viscous dissipation intensifies, the oscillatory behavior shifts from the velocity field toward the temperature field. The impact of the reaction-rate parameter on the local Sherwood number is depicted in Fig. 10; an increase in the reaction-rate parameter enhances the Sherwood number. This behavior is associated with a reduction in concentration near the wall, which produces a steeper concentration gradient and, therefore, greater mass transfer.

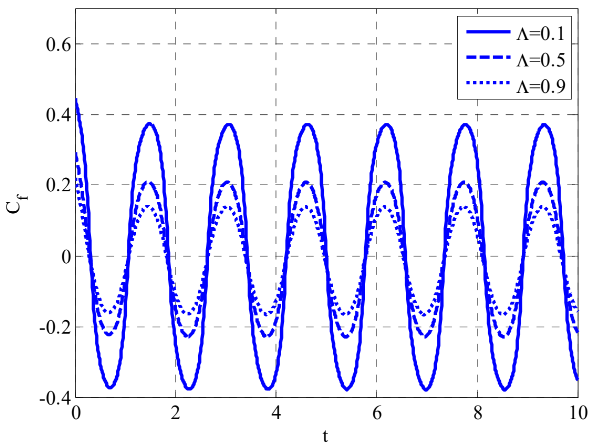

Figure 8. Effect of velocity slip parameter on skin friction coefficient using $S = 1, Da = 0.3, M = 0.1, \lambda = 3, \mathrm{Fr} = 2, Re = 5, Gr_T = 0.1, Gr_C = 0.1, \gamma = 0.5, Pr = 3, Sc = 3, Ec = 10, Bi = 9, N_y = 75, N_t = 1050,\ u(t, 0) = cos(4t) + \Lambda\frac{\partial u}{\partial y}$

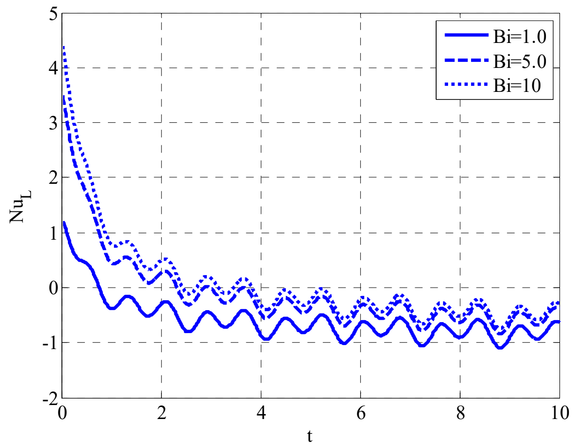

Figure 9. Effect of Biot number on local Nusselt number using $S = 1, Da = 0.3, M = 0.1, \lambda = 3, \mathrm{Fr} = 2, Re = 5, Gr_T = 0.1, Gr_C = 0.1, \gamma = 0.5, Pr = 3, Sc = 3, Ec = 10, \Lambda = 0.9, N_y = 75, N_t = 1050,\ u(t, 0) = cos(4t) + \Lambda\frac{\partial u}{\partial y}$

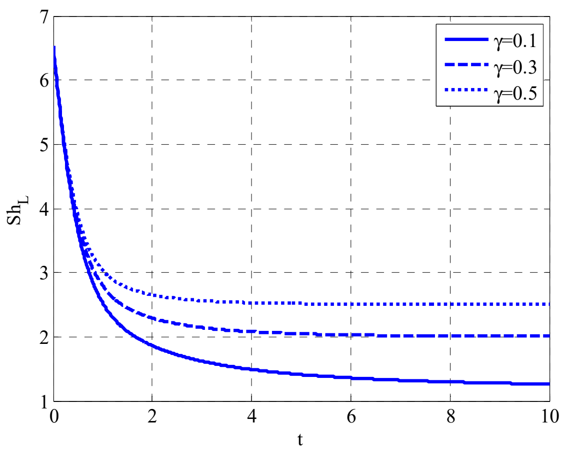

Figure 10. Effect of reaction rate parameter on local Sherwood number using $S = 1, Da = 0.3, M = 0.1, \lambda = 3, \mathrm{Fr} = 2, Re = 5, Gr_T = 0.1, Gr_C = 0.1, \mathrm{Bi} = 9, Pr = 3, Sc = 3, Ec = 10, \Lambda = 0.9, N_y = 75, N_t = 1050,\ u(t, 0) = cos(4t) + \Lambda\frac{\partial u}{\partial y}$

Figures 11–13 display contour plots of velocity, temperature, and concentration fields, along with their respective error distributions. Numerical results are also obtained using the MATLAB **pdepe** solver, which serves as a reference solution in the absence of an analytical benchmark. The error contours are constructed by computing the absolute difference between the solutions generated by the proposed numerical scheme and those obtained from **pdepe**. Figure 14 summarizes the computational time required by the proposed method for the present problem.

For making comparison of the schemes,first stage of propsed scheme using $a_1 = -30$ is used and second and third stages of existing third order Runge-Kutta scheme are used. Existing third order Runge-Kutta scheme is given as

$$\bar{g}_j^{n+1} = g_j^n + \Delta t \left.\frac{\partial g}{\partial t}\right|_j^n$$

$$\bar{\bar{g}}_j^{n+1} = \frac{3}{4} g_j^n + \frac{1}{4}\bar{g}_j^{n+1} + \frac{1}{4}\Delta t \left.\frac{\partial \bar{g}}{\partial t}\right|_j^{n+1}$$

$$g_j^{n+1} = \frac{1}{3} g_j^n + \frac{2}{3}\bar{\bar{g}}_j^{n+1} + \frac{2}{3}\Delta t \left.\frac{\partial \bar{\bar{g}}}{\partial t}\right|_j^{n+1}$$

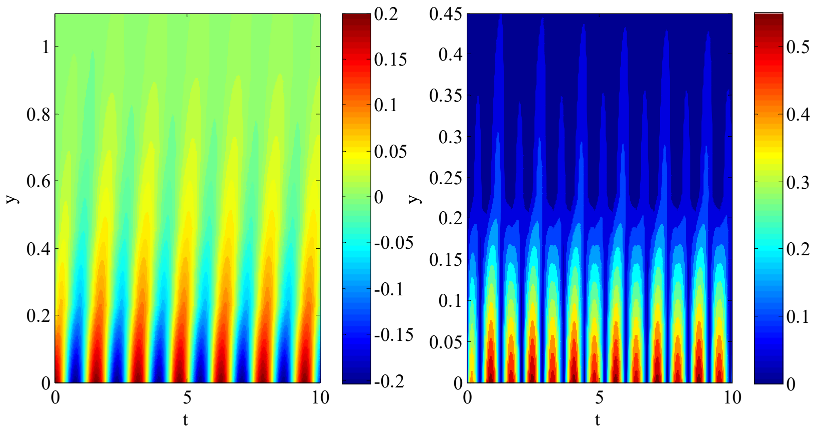

Figure 11. Contour plots for velocity profile and its error using $S = 1, Da = 0.3, M = 0.1, \lambda = 3, \mathrm{Fr} = 2, Re = 5, Gr_T = 0.1, Gr_C = 0.1, \mathrm{Bi} = 9, Pr = 3, \gamma = 0.5, Sc = 3, Ec = 10, \Lambda = 0.9, N_y = 75, N_t = 1050,\ u(t,0) = cos(4t) + \Lambda\frac{\partial u}{\partial y}$

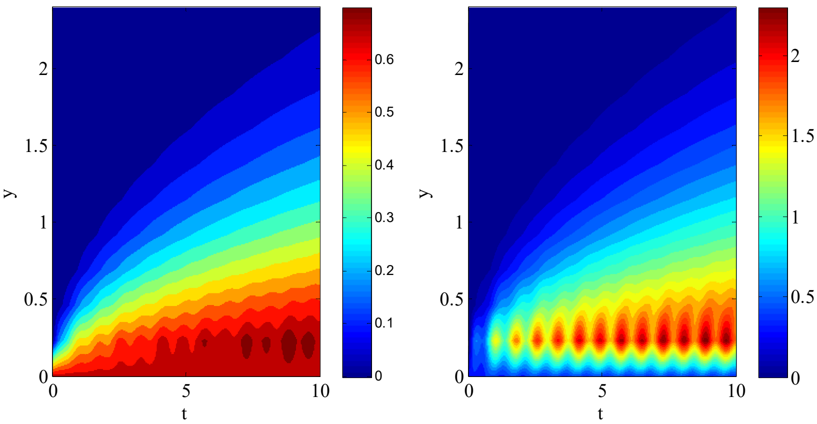

Figure 12. Contour plots for temperature profile and its error using $S = 1, Da = 0.3, M = 0.1, \lambda = 3, \mathrm{Fr} = 2, Re = 5, Gr_T = 0.1, Gr_C = 0.1, \mathrm{Bi} = 9, Pr = 3, \gamma = 0.5, Sc = 3, Ec = 10, \Lambda = 0.9, N_y = 75, N_t = 1050,\ u(t,0) = cos(4t) + \Lambda\frac{\partial u}{\partial y}$

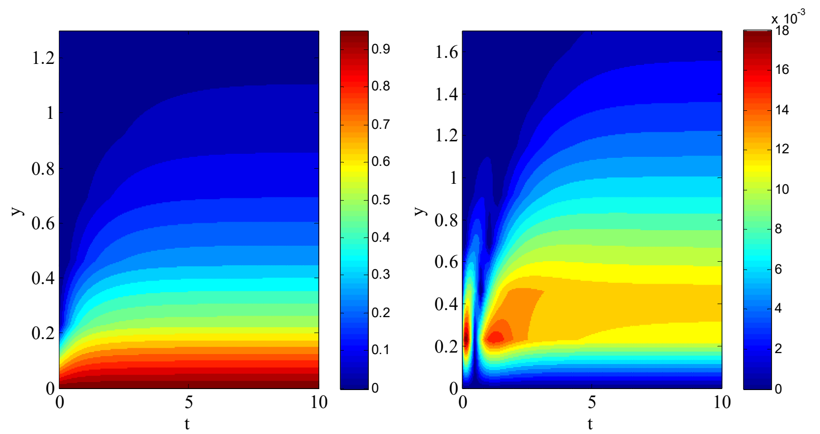

Figure 13. Contour plots for concentration profile and its error using $S = 1, Da = 0.3, M = 0.1, \lambda = 3, \mathrm{Fr} = 2, Re = 5, Gr_T = 0.1, Gr_C = 0.1, \mathrm{Bi} = 9, Pr = 3, \gamma = 0.5, Sc = 3, Ec = 10, \Lambda = 0.9, N_y = 75, N_t = 1050,\ u(t,0) = cos(4t) + \Lambda\frac{\partial u}{\partial y}$

Fig. 15 shows the comparison of the two schemes for second example of convection diffusion problem given in [25]. The error produced by the proposed scheme is less than that obtained by existing third order Runge-Kutta method. The space dependent terms are discretized by the second order central difference scheme. The error is identified by calculating the norm of the difference between the numerical and exact solutions.

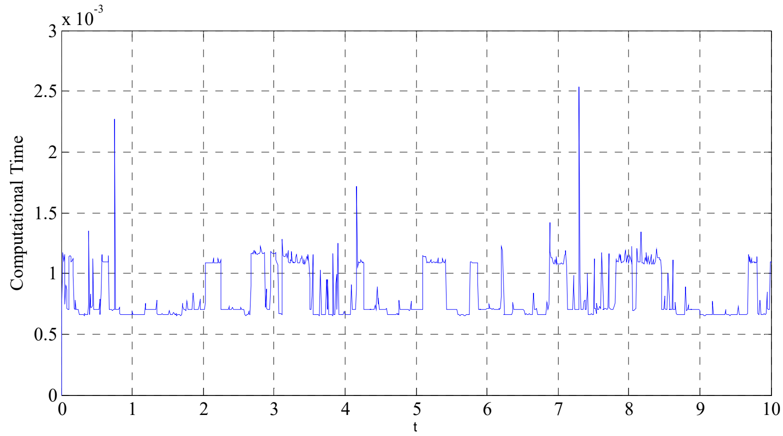

Figure 14. Computational time of the proposed scheme using $S = 1, Da = 0.3, M = 0.1, \lambda = 3, \mathrm{Fr} = 0.1, Re = 5, Gr_T = 0.1, Gr_C = 0.1, \mathrm{Bi} = 5, Pr = 3, \gamma = 0.9, Sc = 3, Ec = 5, \Lambda = 1, N_y = 75, N_t = 1050,\ u(t,0) = cos(4t) + \Lambda\frac{\partial u}{\partial y}$

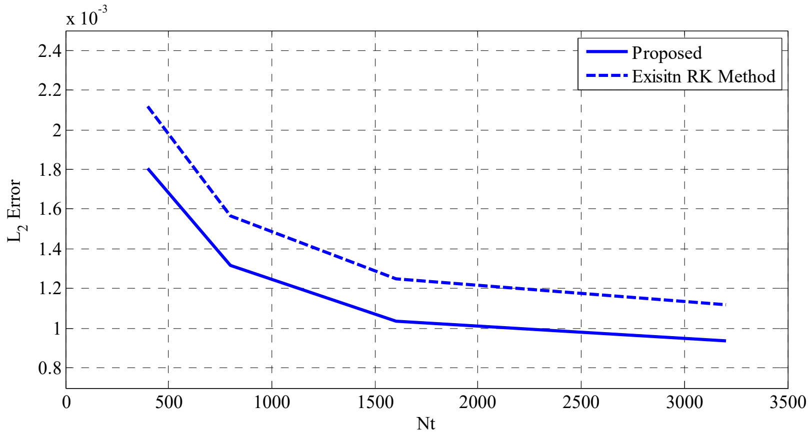

Figure 15. Comparison of two schemes using $t_f = 0.05, N_x = 50, N_t = 400, 800, 1600, 3200$

Table 1 & 2 show grid convergence analysis of proposed and existing Runge-Kutta methods for solving Stokes first problem. Time discretization is done with existing and proposed Runge-Kutta methods. Propsoed scheme performs better than existing third order Runge-Kutta method. Again, for making this comparison, combination of first stage of proposed scheme and second and third stages of third order existing Runge-Kutta method is applied.

Table 1. Grid convergence analysis for Stoeks first problem using $\Delta t = 0.0020$

Δx	a	L_2 Error	
		Proposed	Existing RK
0.3684	40	0.1537	0.1559
0.2414	30	0.1012	0.1021
0.1795	20	0.0756	0.0761
0.1429	9	0.0601	0.0604
0.1186	7	0.0467	0.0469

Table 2. Convergence analysis for Stoeks first problem using $\Delta x = 0.1429$

Δt	a	L_2 Error	
		Proposed	Existing RK
0.0112	−320	0.7680	Diverges
0.0092	−180	0.5885	Diverges
0.0078	−30	0.1320	Diverges
0.0067	3	0.0258	0.0260
0.0059	5	0.0238	0.0240

CONCLUSIONS

A numerical scheme was modified by combining exponential integrator and Runge-Kutta method. Instead of using Euler method in first stage of Runge-Kutta method, exponential integrator is considered. The weights in the numerical scheme for the second and third stages are chosen using the Taylor series. Since, the terms of Taylor series until third order derivative are cancelled out, therefore theoretically scheme provided third order accurate solution in time. For discretizing space dependent terms, compact scheme is chosen. The compact scheme provided high order accuracy in space. The scheme has been applied to problem of flow over the Rige plate and the concluding points can be expressed as

- The velocity profile declined by increasing Eyring number and velocity profile was escalated by incrementing the Darcy number
- The local Nusselt number increases with rising Biot number.
- Local Sherwood number raised by growing reaction rate parameter.
- One of the proposed scheme performed better than existing Runge-Kutta scheme on specific time and space step sizes.

Declarations
Ethical approval and consent to participate
Ethics and Consent to Participate declarations: not applicable.
Consent to Publication
Consent to Publish declaration: not applicable.
Competing interests
The authors declare no competing interests.
Clinical trial number
Clinical trial number: not applicable.
Author Contribution
Writing, Original Draft, Software, Methodology, Analysis Y.N, Writing Original Draft and Funding M.S.A and K.A, Visualization M.M

Acknowledgement: The authors wish to express their gratitude to Prince Sultan University for facilitating the publication of this article through the Theoretical and Applied Sciences Lab.
Funding Statement: The authors would like to acknowledge the support of Prince Sultan University for paying the article processing charges (APC) of this publication.

ORCID
Yasir Nawaz, https://orcid.org/0000-0002-7048-574X; **Muhammad Shoaib Arif,** https://orcid.org/0000-0002-6009-5609
Muavia Mansoor, https://orcid.org/0009-0003-8803-6170; **Kamal Abodayeh,** https://orcid.org/0000-0003-0735-6520

REFERENCES

[1] Y. Nawaz, "Variational iteration method and homotopy perturbation method for fourth-order fractional integro-differential equations.," Computers & Mathematics with Applications, **61**(8), 2330-2341 (2011). https://doi.org/10.1016/j.camwa.2010.10.004
[2] Y. Nawaz, "Development of new and modified numerical methods for hyperbolic conservation laws," Numerical Heat Transfer, Part B: Fundamentals, **76**(4), 224-251 (2019). https://doi.org/10.1080/10407790.2019.1665443
[3] J. C. Butcher, *Numerical Methods for Ordinary Differential Equations*, 2nd ed. (John Wiley & Sons, 2008).
[4] E. Hairer, & G. Wanner, *Solving Ordinary Differential Equations II: Stiff and Differential-Algebraic Problems*, 2nd ed. (Springer Berlin, Heidelberg, 1996).
[5] J. Martín-Vaquero, & B. Janssen, "Second-order stabilized explicit Runge–Kutta methods for stiff problems," Comput. Phys. Commun. **180**, 1802–1810 (2009). https://doi.org/10.1016/j.cpc.2009.05.006
[6] L.M. Skvortsov, "Explicit stabilized Runge-Kutta methods," Computational Mathematics and Mathematical Physics, **51**(7), 1153-1166 (2011). https://doi.org/10.1134/s0965542511070165
[7] G.-D. Hu, and Z. Wang, "A modified Runge–Kutta method for increasing stability properties," Journal of Computational and Applied Mathematics, **441**, 115698 (2024). https://doi.org/10.1016/j.cam.2023.115698
[8] A. Abdulle, "Fourth order Chebyshev methods with recurrence relation," SIAM Journal on Scientific Computing, **23**(6), 2041-2054 (2002). https://doi.org/10.1137/s1064827500379549
[9] B. Kleefeld, and J. Martín-Vaquero, "SERK2v2: A new second-order stabilized explicit Runge-Kutta method for stiff problems," Numerical Methods for Partial Differential Equations, **29**(1), 170-185 (2013). https://doi.org/10.1002/num.21704
[10] M. Z. Liu, M. H. Song, and Z. W. Yang, "Stability of Runge–Kutta methods in the numerical solution of equation u′(t)= au (t)+ a0u ([t])," Journal of Computational and Applied Mathematics, **166**(2), 361-370 (2004). https://doi.org/10.1016/j.cam.2003.04.002
[11] R. K. Alexander, "Stability of Runge–Kutta methods for stiff ordinary differential equations," SIAM journal on numerical analysis, **31**(4), 1147-1168 (1994). https://doi.org/10.1137/0731060
[12] E. C. Emmanuel, N. Chidinma, and N. Ifeoma, "On Review of the Convergence Analyses of the Runge Kutta Fixed Point Iterative Methods," Asian Journal of Pure and Applied Mathematics, **2**(1), 20-44 (2020).

[13] A. V. Shenoy, "Darcy-Forchheimer natural, forced and mixed convection heat transfer in non-Newtonian power-law fluid-saturated porous media," Transport in porous media, **11**(3), 219-241 (1993). https://doi.org/10.1007/bf00614813
[14] Z. Shah, A. Shafiq, M. Rooman, M. H. Alshehri, and E. Bonyahet, "Darcy Forchhemier Prandtl-Eyring nanofluid flow with variable heat transfer and entropy generation using Cattaneo-Christov heat flux model: Statistical approach," Case Studies in Thermal Engineering, **49**, 103376 (2023). https://doi.org/10.1016/j.csite.2023.103376
[15] S. Chaudhary, and K. K. Chouhan, "Darcy-Forchheimer flow of Prandtl-Eyring nanofluid subjected to a Riga plate of varying thickness along with Brownian diffusion, thermophoresis and non-uniform heat source/sink effects," Numerical Heat Transfer, Part A: Applications, **84**(7), 732-759 (2023). https://doi.org/10.1080/10407782.2022.2154725
[16] Z. Ullah, I. Ullah, G. Zaman, H. Khan, and T. Muhammad, "Mathematical modeling and thermodynamics of Prandtl–Eyring fluid with radiation effect: a numerical approach," Scientific Reports, **11**(1), 22201 (2021). https://doi.org/10.1038/s41598-021-01463-4
[17] A. Baidya, S. Mukhopadhyay, and G. C. Layek, "Melting heat transfer in Eyring–Prandtl fluid flow past a nonlinear stretching sheet in presence of slip," Canadian Journal of Physics, **103**(10), 968-977 (2025).
[18] M. Awais, T. Salahuddin, and S. Muhammad, "Effects of viscous dissipation and activation energy for the MHD Eyring-powell fluid flow with Darcy-Forchheimer and variable fluid properties," Ain Shams Engineering Journal, **15**(2), 102422 (2024). https://doi.org/10.1016/j.asej.2023.102422
[19] A. Ajibade, and P. O. Ojeagbase, "Effect of viscous dissipation on seady natural convection heat and mass transfer in a vertical channel with variable viscosity and thermal conductivity," Journal of Heat and Mass Transfer Research, **7**(2), 105-116 (2020). https://doi.org/10.1002/eng2.12268
[20] O. Mahitha, and V.K.A. Golla, "Magnetite/engine oil Casson nanofluid flow over a Riga plate with Atangana–Baleanu fractional derivative," Case Studies in Thermal Engineering, **52**, 103712 (2023). https://doi.org/10.1016/j.csite.2023.103712
[21] M. Bilal, F. Maiz, M. Farooq, H. Ahmad, M. Kh. Nasrat, and H. A. Ghazwani, "Novel numerical and artificial neural computing with experimental validation towards unsteady micropolar nanofluid flow across a Riga plate," Scientific Reports, **15**(1), 759 (2025). https://doi.org/10.1038/s41598-024-84480-3
[22] R. Reyaz, A. Q. Mohamad, L. Y. Jiann, M. Saqib, and S. Shafie, "Presence of Riga plate on MHD Caputo Casson fluid: an analytical study," J. Adv. Res. Fluid Mech. Therm. Sci, **93**(2), 86-99 (2022). https://doi.org/10.37934/arfmts.93.2.8699
[23] J. Martin-Vaquero, and B. Janssen, "Second-order stabilized explicit Runge–Kutta methods for stiff problems," Computer Physics Communications, **180**(10), 1802-1810 (2009). https://doi.org/10.1016/j.cpc.2009.05.006
[24] J. Li, and Y.-T. Chen, *Computational partial differential equations using MATLAB*®, (CRC press, 2019).
[25] D. A. Koç, Y. Öztürk, and M. Gülsu, "A numerical algorithm for solving one-dimensional parabolic convection-diffusion equation," Journal of Taibah University for Science, **17**(1), 2204808, (2023). https://doi.org/10.1080/16583655.2023.2204808

МОДИФІКОВАНА СХЕМА РУНГЕ-КУТТИ ТА КОМПАКТНА ПРОСТОРОВА СХЕМА ДЛЯ ПОТОКУ РІДИНИ ПРАНДТЛЯ-ЕЙРІНГА ЗА МЕТОДАМИ ДАРСІ ФОРХГАЙМЕРА НАД РИГА ПЛАСТИНОЮ

Ясір Наваз[1], Мухаммад Шоайб Аріф[2], Муавія Мансур[3], Камал Абодайє[2]
[1]*Кафедра математики, Факультет інженерії та обчислювальної техніки, Національний університет сучасних мов (NUML), Ісламабад, 44000, Пакистан*
[2]*Кафедра математики та природничих наук, Коледж природничих наук та гуманітарних наук, Університет Принца Султана, Ер-Ріяд, 11586, Саудівська Аравія*
[3]*Кафедра математики, Університет Ваха, Вах Кантт 47040, Пакистан*

Запропоновано модифікацію існуючого методу Рунге-Кутти третього порядку. Схема є явною, а її перший етап складається з нестандартного знаменника, тоді як останні два етапи такі ж, як і у методу Рунге-Кутти. Для дискретизації просторово-залежних членів використовується компактна схема високого порядку. Запропонована схема з просторовою дискретизацією використовується для знаходження умови стійкості запропонованої схеми. Схема застосовується до безрозмірної моделі у вигляді диференціальних рівнянь з частинними похідними для ковзного потоку неньютонівської рідини над рига пластиною з тепло- та масообміном. За допомогою запропонованої схеми отримано різні типи графіків для профілів швидкості, температури та концентрації. Деякі результати, отримані за запропонованою схемою, порівнюються з результатами, отриманими за допомогою числового розв'язування за допомогою розв'язувача MATLAB PDEPE. Схема також порівнюється з існуючою схемою Рунге-Кутти третього порядку, і вона дає точніші результати, ніж існуюча схема, при певних розмірах кроку в часі та просторі.

Ключові слова: *гібридна схема; стійкість; конвергенція; ковзаючий потік; рідина Ейрінга-Прандтля*